Polymer 334 (2025) 128695

Contents lists available at ScienceDirect

Polymer

journal homepage: www.elsevier.com/locate/polymer

Thermally sensitive and tunable water-soluble polymer molds for the preparation of porous hydrogels

Lisa Delattre [a], Arthur Lassus [a], Gregory De Crescenzo [b], Nathalie Faucheux [c], Marc-Antoine Lauzon [c], Benoît Paquette [d], Mélanie Girard [a], Nick Virgilio [a,*]

[a] Research Center for High Performance Polymer and Composite Systems (CREPEC), Department of Chemical Engineering, Polytechnique Montréal, Montréal, H3C 3A7, Québec, Canada
[b] Department of Chemical Engineering, Polytechnique Montréal, Montréal, H3C 3A7, Québec, Canada
[c] Department of Chemical Engineering and Biotechnological Engineering, Faculty of Engineering, Université de Sherbrooke, J1K 2R1, Sherbrooke, Québec, Canada
[d] Center for Research in Radiotherapy, Department of Nuclear Medicine and Radiobiology, Faculty of Medicine and Health Sciences, Université de Sherbrooke, Sherbrooke, J1H 5N4, Québec, Canada

ARTICLE INFO

Keywords:
Polyvinyl alcohol
Porous hydrogel
Co-continuous polymer systems

ABSTRACT

Porous hydrogels are highly sought-after biomaterials for regenerative medicine and 3D cell culture media. For such purposes, direct contact between the hydrogels and organic solvents during the synthesis step must be avoided as much as possible. In this work, porous water-soluble molds, composed of a thermosensitive and melt-processable, i.e. thermoplastic, polyvinyl alcohol (PVA), are used to prepare porous hydrogels. The process offers a high level of control over the porosity features, including full pore interconnectivity and tunable average pore size from nearly 75 μm to 200 μm – the typically targeted range for cell growth in a 3D scaffold. The porous PVA molds are prepared by the sequential process of (1) melt-extrusion of a polystyrene (PS)/PVA co-continuous blend, (2) quiescent annealing to tune the morphology, (3) and selective extraction of the PS phase. The gelling solution is injected in the PVA molds at low temperature – i.e. < 50 °C when the molds are insoluble. Once the solution has gelled, the PVA molds are extracted in hot water – i.e. > 50 °C, over which the molds are fully water soluble, yielding porous hydrogels with nearly comparable macroscopic and microscopic features to the PVA molds, as revealed by electron microscopy and microcomputed tomography. The approach is demonstrated herein with sodium alginate hydrogels, and could be extended to other types of gel chemistries.

1. Introduction

Porous hydrogels combine a variety of sought-after properties in fields of applications such as regenerative medicine [1], 3D cell culture media (e.g. for drug screening) [2,3], monoliths for heterogeneous catalysis [4], actuators [5], water filtration [6], cancer treatment [7], etc. They are soft, easily deformable and display viscoelastic properties comparable to tissues. They offer a 3D environment reminiscent of the extracellular matrix for cell culture [8], high permeability allowing diffusion of molecular compounds in and out of the gel phase, macropores allowing the flow of liquids in and out of the material and the migration of cells deep within the material, in addition to the efficient transport of oxygen, nutrients and wastes for 3D cell culture. Finally, they offer a variety of functional groups available for (bio)functionalization [9], and they are capable of absorbing species such as heavy metallic ions [10], and immobilizing catalytic nanoparticles [4].

All of these applications require a finely tuned network of interconnected macropores characterized by their size distribution (and average size), volume fraction, specific surface, and surface functionality, in addition to the hydrogel chemistry itself. The variety of applications means that wide ranges of porosity values and gel chemistries are necessary to meet the constraints associated with each application. As a result, several techniques exist to synthesize porous hydrogels: templating based on the dissolution of a salt or porogen phase (i.e. NaCl particulates, gelatin microspheres) embedded in the hydrogel during synthesis [11,12]; gas foaming, creating cavities in the hydrogel by a chemical or physical process generating gas bubbles [13,14]; cryogelation involving phase separation of a liquid phase containing a gelling agent, and ice crystals forming upon cooling of the material [15,16]; the constantly expanding families of 3D printing [17], and

* Corresponding author.
E-mail address: nick.virgilio@polymtl.ca (N. Virgilio).

https://doi.org/10.1016/j.polymer.2025.128695
Received 9 February 2025; Received in revised form 22 May 2025; Accepted 16 June 2025
Available online 17 June 2025
0032-3861/© 2025 The Authors. Published by Elsevier Ltd. This is an open access article under the CC BY-NC license (http://creativecommons.org/licenses/by-nc/4.0/).

stereolithographic techniques [18], to name a few.

Porous hydrogels prepared with porous polymer molds obtained from melt-processed co-continuous polymer blends belong to the porogen templating technique [19]. Briefly, a co-continuous polymer blend, composed of intertwined and fully continuous phases of two immiscible polymers, is prepared by melt-processing (i.e. melt-extrusion or equivalent melt-processing technique) [20]. Following processing, quiescent annealing over the glass/melting temperature can be used to let the morphology coarsen to the desired length scale – typically from a few μm, to nearly 1000 μm [21]. Next, the selective extraction of one polymer phase with a solvent yields porous polymer monoliths. These monoliths are filled with a gelling solution and after gelation, the polymer mold is extracted with a selective solvent – most often an organic solvent [19]. Overall, this method yields porous hydrogels with fully interconnected pores, with a volume fraction typically ranging from 40 % to 60 %, and an average pore size ranging from a few μm to nearly 600 μm and possibly more. Finally, this technique is compatible with numerous gel chemistries [7,22,23].

As explained, the last extraction step typically uses an organic solvent to remove the polymer mold (e.g. chloroform, toluene, etc.). While these solvents do not necessarily pose a particular problem for certain types of applications (e.g. catalysis), they do pose issues when it comes to biomaterials and their applications, such as cell culture or regenerative medicine, if traces of solvent are present within the macroporous gels. In all cases, reducing the use of organic solvents is always desirable for health and processing concerns. An alternative to avoid the use of organic solvents would be to use water-soluble polymer molds. Kabbara et al. successfully prepared porous organogels (an organic solvent immobilized by an organogelator) using polyvinyl alcohol (PVA) molds prepared from PVA/poly (ε-caprolactone) (PCL) co-continuous melt-processed blends. Since PVA is a water soluble polymer, they were able to use water to remove the porous PVA mold after gelation, avoiding direct contact of the organogel with an organic solvent [23].

Organogels are oil or solvent based gels which do not readily dissolve PVA when in direct contact. However, it would be desirable to use a similar approach to produce hydrogels, which are water-based – without provoking the immediate dissolution of the PVA mold upon contact with the aqueous solution containing the gelling agent.

The main objective of this work was to develop a process to prepare macroporous hydrogels using water-soluble molds, by retarding or inhibiting the dissolution of the molds until gelation has occurred – i.e. by using a temperature sensitive water-soluble polymer. PVA remains a good option since its solubility in water, as a function of temperature, can be tuned by adjusting the level of hydrolysis of polyvinyl acetate [24,25] – a higher level of hydrolysis typically yielding a less soluble PVA due to stronger interchain hydrogen bonding. In addition, the selected grade of PVA must be melt-processable (i.e. a thermoplastic PVA) to prepare a co-continuous blend with a complementary immiscible polymer. The strategy would be next to inject the gelling solution in the PVA mold in a range of temperature over which the PVA is insoluble in water, and next rapidly change the temperature in a range over which the PVA becomes soluble, to let the mold dissolve, yielding porous hydrogels without any contact with an organic solvent.

2. Experimental section

2.1. Materials and methods

A flowchart detailing the sequence of experiments including materials characterization, polymer blends preparation and characterization, and porous hydrogel preparation and characterization, is displayed in Scheme S1.

2.1.1. Materials

Polystyrene (PS, pellet form) MC3650 was purchased from Americas Styrenics. Thermoplastic polyvinyl alcohol (PVA, pellet form) Mowiflex™ M05 was obtained from Kuraray America Inc. Chloroform of HPLC grade was obtained from Fisher Chemical. Anhydrous ethanol was purchased from Greenfield Global Les Alcools de Commerce. Sodium alginate (SA, grade IL-6 G) was obtained from the Kimica Corporation (M/G ratio = 0.5, η = 30–60 mPa s (1 %) (from supplier), M_n = 67,000 ± 8000 g/mol [26]). Calcium chloride (100035-04-8) was purchased from Sigma-Aldrich. Chitosan (CHI) 85/60/A1 was obtained from Bio-Log Heppe GmbH, Landsberg, Germany, with the following properties: degree of deacetylation (DDA) = 85 %, viscosity: 60 mPa s, Mn = 50–100 kDa (from supplier). Genipin (GNP) (Mw = 226.23 g mol−1, purity >98 %) was purchased from Thermo Fisher Scientific. Sodium bicarbonate ($NaHCO_3$, #S6014, 99.7 % purity) was purchased from Sigma-Aldrich.

2.1.2. Density measurements

Density measurements were realized with a PvT-100 instrument from ThermoHaake. Briefly, 0.8–1 g of PVA or PS was first introduced in the instrument. Then, three pressure values were applied to the materials: 150, 225, and 300 bar. For each pressure, the temperature was varied from 220 °C to 20 °C, at an increment ΔT of 50 °C and at a cooling rate of 25 °C/min. Throughout the process, the instrument measures the volume occupied by the material. From the measured P-V-T curves, the density of the material at atmospheric pressure at both 20 °C and 210 °C were obtained by extrapolation. In this work, three tests were conducted for each material to obtain the average density values reported in Table 1.

2.1.3. Differential scanning calorimetry

The thermal properties of the materials including the glass transition temperature (T_g), melting temperature (T_m) and crystallization temperature (T_c), were measured by differential scanning calorimetry (DSC) using a TA Instruments Q2000 instrument. The following protocol was employed: (1) equilibrium at −90 °C; (2) heating from −90 °C to 240 °C at 10 °C/min; (3) cooling from 240 °C to −90 °C at 10 °C/min; (4) second heating from −90 °C to 240 °C at 10 °C/min. Following this protocol, the thermograms were analyzed using the TA Universal Analysis software. The binary blends were also analyzed to assess the miscibility of the polymers by observing shifts in the Tg values as a function of composition. The thermal properties of the pure materials are presented in Table 1.

2.1.4. Rheology

For the rheological tests, discs with a diameter of 25 mm and a thickness of 2 mm were prepared from neat PS and PVA pellets using a hot press. The polymers were initially dried for 24 h at 70 °C under vacuum. The pellets were placed in a mold and pressed at 5000 lbs for 5 min at 190 °C for PS, and 210 °C for PVA. Three types of rheological tests were conducted for each polymer: (1) amplitude sweep (to determine the linear viscoelastic region), (2) time sweep (stability of the material at high temperature, Fig. S1), and (3) frequency sweep (to measure the complex viscosity $|\eta^*|$). These tests were realized using a MCR 302 stress-controlled rheometer from Anton Paar equipped with a CTD 450

Table 1
Density and thermal properties of PS and PVA.

Polymers	T_g [b] [°C]	T_m [b] [°C]	$\rho(20°C)$ [c] [g/cm³]	$\rho(210°C)$ [c] [g/cm³]	$\lvert\eta^*\rvert$ (220°C) [d] [Pa/s]
PVA	49 45[a]	191 195[a]	1.23 ± 0.01 0.6-0.9[a]	1.14 ± 0.01	543 ± 34
PS	95 94[a]	–	1.01 ± 0.01 1.04[a]	0.93 ± 0.01	1224 ± 22

[a] Supplier data.
[b] Measured by DSC.
[c] Measured by PvT.
[d] Measured by rheometry.

oven and a 25 mm diameter parallel plate geometry, at 220 °C under nitrogen. Amplitude sweep tests were realized at 10 rad/s from $\gamma_0 =$ 0.01 %–700 %. Frequency sweeps were realized at $\gamma_0 = 1$ %: (1) for PVA, from 1 rad/s to 100 rad/s and from 0.5 rad/s to 100 rad/s due to polymer instability at 220 °C; (2) for PS, from 0.1 rad/s to 100 rad/s. Zero-shear viscosities were determined using the Carreau-Yasuda model. Each test was performed three times for each polymer. The validity of the Cox-Merz rule was assumed to be valid for both tested polymers.

2.1.5. Thermogravimetric analysis

The polymers were initially dried for 24 h at 70 °C under vacuum. The thermal stability of the materials as a function of temperature was monitored by thermogravimetric analysis (TGA) using a 5500 instrument from TA Instruments using a 10 °C/min ramp. The results are presented in Fig. S2.

2.2. Solubility of PVA

The solubility of PVA in water as a function of time and temperature was evaluated at 10 °C, 23 °C, 50 °C, and 70 °C. For each temperature, three samples were weighed every 30 min over a period of 8 h. The mass variation was calculated according to Equation (1), where *m(t)* is the mass of the sample at time *t*, and *m(0)* is the initial mass of the sample:

$$p = \frac{m(t) - m(0)}{m(0)} \quad \text{Equation 1}$$

2.3. Interfacial tension measurement

The interfacial tension between the two polymers was measured using the breaking thread method. PS films were prepared by pressing pellets at 190 °C and 10,000 lbs in a heated press during 5 min. The film thickness was measured in-between 100 and 300 μm. PVA filaments were manually prepared by heating a pellet at approx. 220 °C, then by pulling fine filaments with tweezers - the filaments had a diameter of 25–55 μm. Next, a PVA filament was sandwiched between two PS films and placed on a glass microscope slide, then covered with a glass coverslip. This assembly was inserted into a Mettler FP-82HT hot stage controlled by a Mettler FP-90 Central Processor at 220 °C. The periodic sinusoidal deformation of the PVA filament was monitored with an optical microscope (Nikon instrument) connected to a computer for image capture via a Coreco Oculus image analysis system and Visilog 4.1.3 software. The images were subsequently processed using the ImageJ 1.53 software to measure the deformation amplitude of both minimum and maximum filament diameters as a function of time, and the wavelength associated to the periodic deformation. According to Tomotika's theory, the interfacial tension (σ) is calculated using Equations (2)–(4):

$$\sigma = \frac{q\eta_{PS}D_0}{\Omega(\lambda, p)} \quad \text{Equation 2}$$

$$q = \frac{\ln\left(\frac{\alpha(t)}{\alpha_0}\right)}{t} \quad \text{Equation 3}$$

$$\frac{\alpha(t)}{\alpha_0} = \frac{D_{max}(t) - D_{min}(t)}{D_{max}(t_0) - D_{min}(t_0)} \quad \text{Equation 4}$$

where η_{PS} is the zero-shear viscosity of PS (Table 1), D_0 is the initial diameter of the PVA filament, and $\Omega(\lambda, p)$ is a function tabulated in Chappelear's article [27], where λ is the average wavelength, and p is the ratio between the zero-shear viscosity of PS and the zero-shear viscosity of PVA (Table 1). $D_{max}(t)$ and $D_{min}(t)$ represent the average maximum and minimum filament diameters at time *t*, respectively. The value of q used to calculate the interfacial tension is the average of three values for each time *t*. $\alpha(t)$ is the difference between the maximum and minimum diameters at time *t*, and α_0 is the initial difference at a chosen time t_0.

2.4. Blend preparation

2.4.1. Internal mixer

Binary blends of PS/PVA were prepared over the whole composition spectrum using an internal mixer Thermohaake Rheodrive 7 kW coupled with the Rheomix 600 mixing chamber. First, the pure polymers were dried under vacuum at 70 °C for 24 h. Then, the desired amounts of polymers were introduced into the internal mixer, which was set at a temperature of 210 °C (blend temperature reached approx. 216 °C during mixing due to viscous dissipation). The total polymer volume was 50 cm^3. Mixing was carried out for 6 min under a nitrogen atmosphere at 50 rpm. The blends were rapidly quenched in a bath of ethanol and dry ice to freeze-in the morphology.

2.4.2. Melt-extrusion

Melt-extrusion was next employed to prepare larger quantities of PVA molds with nearly identical characteristics [28,29]. The PS/PVA blend (61/39 vol%) was extruded using an AG 34 mm Leistritz co-rotating twin-screw extruder. The pure materials were first dried under vacuum at 70 °C for 24 h. Subsequently, 3.8 kg of the blend was prepared, consisting in 2.1 kg of PS and 1.7 kg of PVA. The mixed granules were introduced into the twin-screw extruder using a feeder at a rate of 7 kg/h and a screw speed of 100 rpm. A temperature profile of 210 °C was maintained throughout the extruder. The filament exiting the extruder was cooled in air and then cut into pellets using a pelletizer (Scheer Bay SB50).

Blend pellets were then processed with a single-screw extruder (Killion KN-150). The temperature profile along the extruder was set at 160 °C–185 °C – 210 °C, with a screw speed of 16 rpm. An extrusion die with a diameter of 11/16 in (17.5 mm) was used to extrude polymer blend rods with a final diameter ranging from 18 to 25 mm. Since the rods are shaped by gravity upon exiting the die, they are not uniform along their entire length; the leading section has a larger diameter than the trailing section. Upon exiting the extruder, the rods were rapidly quenched in a bath of ethanol and dry ice to freeze-in the morphology.

2.4.3. Quiescent annealing

Annealing of co-continuous blends was performed using a hot press. The samples were first wrapped in aluminum foil and then placed between the heated plates of the press, which were maintained at 210 °C. A slight pressure was applied to ensure uniform heating. The samples were kept in the press for 10, 20, 30, 45, or 60 min, depending on the desired annealing time. Finally, the samples were quenched in a bath of ethanol and dry ice to freeze-in the morphology.

2.5. Characterization of blends

2.5.1. Continuity of polymer phases by gravimetry

Gravimetric analysis was employed to measure the continuity of each polymer phase in the blends – for blends prepared both in the internal mixer and by melt-extrusion, right after processing or after quiescent annealing. First, blend pieces were randomly cut into cubes from different locations. The cubes side dimensions did not exceed 2 cm. Each sample was weighed before being plunged in either chloroform (to extract the PS phase) or hot water at 70 °C (to extract the PVA phase). The extraction lasted for 2 weeks, with solvent changes every 2 days. Afterwards, the samples were dried under vacuum for 24 h at 70 °C, and then reweighed. The PS and PVA continuities were calculated using Equations 5 and 6:

$$PS\ continuity\ (\%) = \frac{m_i - m_f}{m_i} * \frac{m_{blend}}{m_{PS\ in\ blend}} * 100\ (for\ chloroform\ extraction)$$

Equation 5

$$PVA\ continuity\ (\%) = \frac{m_i - m_f}{m_i} * \frac{m_{blend}}{m_{PVA\ in\ blend}} * 100\ (for\ water\ extraction)$$

Equation 6

where m_i is the initial mass of the sample, m_f is the final mass of the sample, m_{blend} is the total mass of the blend from which the sample was taken, $m_{PS\ in\ blend}$ is the mass of PS in the blend, and $m_{PVA\ in\ blend}$ is the mass of PVA in the blend. At least three samples per blend and per solvent extraction were analyzed.

2.5.2. Microstructural analysis by scanning electron microscopy

Microstructural analysis of the blends was realized by scanning electron microscopy (SEM, HITACHI Regulus 8220). Samples were first prepared by microtomy at room temperature (Leica RM2165) to obtain a smooth surface. The samples were then plunged in either chloroform to extract the PS phase and observe the remaining PVA phase, or in hot water at 70 °C to extract the PVA and observe the remaining PS phase. The extraction process lasted for 2 weeks, with solvent change every 2 days. Following extraction, the samples were dried under vacuum for 24 h at 70 °C. To complete sample preparation, an 8 nm thick carbon layer was deposited on the surface using a Leica EM ACE600 instrument. Finally, the samples were observed by SEM at an accelerating voltage of 1 kV and a current of 10 μA.

2.5.3. Microstructural analysis by X-ray microtomography

Porosity characterization of co-continuous blends (right after processing or after annealing) was also performed by X-ray microtomography (microCT) with a Zeiss Xradia 520 Versa system. Samples from the internal mixer were cut into cubes with sides not exceeding 2 cm, using a circular saw. Melt-extruded blend samples were machined into cylinders (diameter = 5 mm, height = 6 mm) using a computerized numerical control (CNC) instrument (Genmitsu 3020-PRO MAX Router). The samples were then plunged in chloroform for 2 weeks to extract all of the polystyrene, with the solvent being replaced every 2 days. Afterwards, they were dried under vacuum at 70 °C for 24 h. Finally, the samples were analyzed by microCT at 50 kV, 4 W, and 70 μA. A noise reduction filter (NRF) was applied to the images to remove ring artifacts using the Scout-and-Scan Control System Reconstructor software.

Porosity analysis using the microCT images was realized next using the Dragonfly software. Once the images are imported into the software, the first step is to adjust the contrast to obtain a black and white reconstruction, where the pores appear in black and the PVA phase (or gel phase) in white, allowing for the clear distinction between the two phases. Next, the PVA or gel regions are isolated to generate specific masks, and their inverse masks are created to obtain a specific mask for the pores. A cylindrical or cubic cut, depending on the sample shape, is then performed to remove the sample holder, external elements, and aberrant parts of the sample. Finally, an integrated algorithm is used to determine the average domain size and size distributions. It is also possible to calculate the specific pore surface area by taking the total pore surface area and dividing it by the sample volume. These values are also obtained using an integrated algorithm.

2.6. Preparation and characterization of porous gels

2 % or 4 % (w/v) SA aqueous solutions were cooled at 2 °C using an ice bath. Next, porous PVA molds prepared from PS/PVA co-continuous blends (without or with prior annealing) were plunged in the cold solution and placed in a custom-built injection system applying pressure-vacuum cycles. Three pressure-vacuum cycles were applied, after which the mold was quickly removed, and the excess solution absorbed with paper. The filled molds were then placed in a 4 % (w/v) $CaCl_2$ solution at 5 °C overnight. Finally, the filled molds were transferred to a 4 % (w/v) $CaCl_2$ solution at 70 °C to extract all of the PVA. The solution was replaced when it was fully turbid. The extraction time varied from 20 min to one day, depending on the PVA mold pore size and the accessibility of the PVA within the gel phase. The resulting porous gels were then placed back into a 4 % (w/v) $CaCl_2$ solution at room temperature. The 4 % (w/v) SA porous gels were subsequently analyzed by microCT, following the procedure described in Section 2.5.3.

Hydrogels composed of SA, chitosan (CHI) and genipin (GNP, a biobased chemical crosslinker for CHI) were prepared following the protocol of Parès et al. [29]. Aqueous solutions of SA (5 % w/v), GNP (0.3 % w/v), and an aqueous solution of CHI (1.5 % w/v) with $NaHCO_3$ (0.045 % w/v) in 0.1 M acetic acid were first prepared. These solutions were then combined to obtain a final concentration ratio of 2/0.75/0.05 (% w/v). After preparation, the solution was cooled in an ice bath at 2 °C. PVA porous molds were subsequently immersed in the cold mixture and placed under reduced pressure to allow the solution to fully penetrate the molds. The filled molds were then incubated in a humid oven at 37 °C for 24 h to complete the crosslinking process between CHI and GNP. After gelation, the molds were transferred to a 4 % (w/v) $CaCl_2$ solution at 70 °C to extract all of the PVA and crosslink SA with Ca^{2+}.

3. Results

3.1. PVA solubility as a function of temperature

The first step was to evaluate and quantify the swelling and solubility behavior of pure PVA in water as a function of temperature, to determine the range of temperatures compatible with the gel preparation steps: (1) a first range of T over which the PVA is insoluble, to allow for solution injection and gelling in the PVA molds; (2) a second range over which the PVA is fully soluble for the mold extraction step, yielding the porous gels.

Fig. 1a shows that the PVA swells in water and absorbs more than twice its mass at 10 °C and 23 °C, until the samples break after nearly 8 h (475 min) due to extensive handling and fragility of the swollen sample – however, no dissolution is measured. In addition, the swelling rate increases initially as the T increases from 10 °C to 23 °C. Fig. 1b shows how much the PVA swells after 4 h (240 min) in water, with the pellet reaching approximately 3 times its initial size. At 50 °C, after initial swelling, dissolution occurs and at 70 °C, slight swelling is observed, followed by quick dissolution.

One key observation is that the PVA pellet retains its shape during the swelling phase at low temperature, which is an important feature if this material is to be used as a mold to prepare porous hydrogels. In that sense, this PVA displays a thermosensitive behavior: under 50 °C, swelling occurs but there is no dissolution. At 50 °C, there is a transition as dissolution is now observed (weight loss is measured after approx. 100 min), and almost immediately at 70 °C. The ideal approach to inject a gelling solution into a PVA mold would be at a low temperature to prevent mold dissolution (although it will likely swell), then to dissolve it at a higher temperature once the gel has set. The next step then consisted in preparing porous PVA molds.

3.2. Preparation of porous PVA molds from a PS/PVA co-continuous system

Fig. 2 displays the morphology of PS/PVA blends as a function of composition after melt-processing in an internal mixer. The typical features of a binary immiscible system can be observed, with matrix-dispersed phase morphologies at low compositions of PS or PVA (Fig. 2a–c, e-j), and a co-continuous morphology at 61/39 vol% (intermediate composition, Fig. 2d). The DSC thermograms (data not shown) confirm that the PS and PVA phases are immiscible at all compositions, as their respective Tg remain constant and equal to the values of the pure polymers (respectively 95 °C and 49 °C).

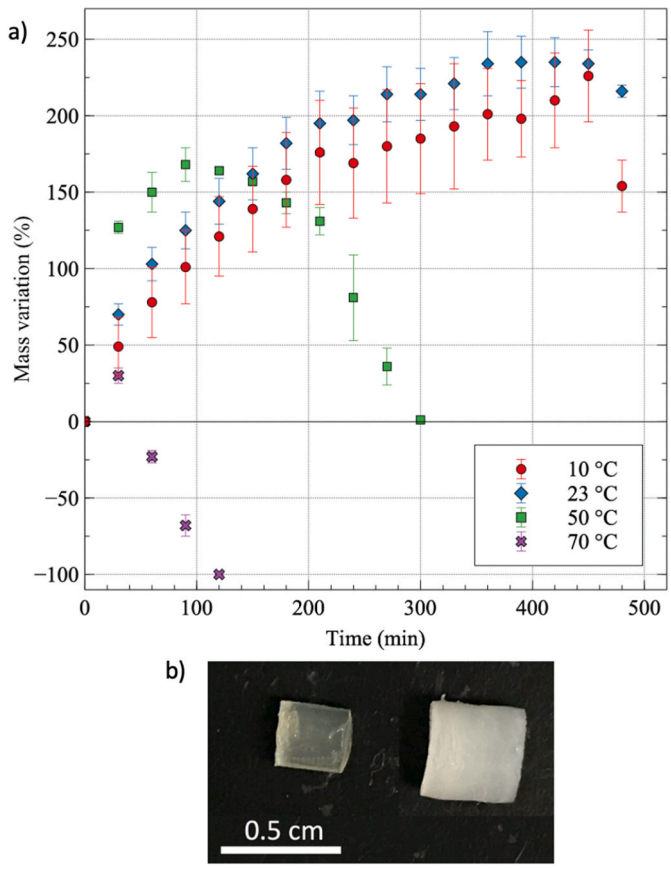

Fig. 1. a) Swelling and dissolution of PVA in water as a function of time and temperature; b) Comparison between a PVA pellet at t = 0 h (dry, left) and after 4 h in water at 23 °C (right).

Fig. 2a–c shows that the PVA dispersed phase increases in size as its composition increases up to 30 % – a similar result is observed when the PS forms the minor phase (Fig. 2f–j), although it is finer compared to the dispersed phase of PVA. There is then a sharp morphological transition observed at 39 % of PVA, with the formation of a co-continuous morphology (Fig. 2d) – with the observation of PS sub-inclusions in the PVA phase, and vice-versa (see Fig. S2a). Slightly increasing the PVA composition to 40 % results in the formation of a PVA matrix comprising PS droplets – with very small cavities within the extracted droplets linking neighboring droplets and creating a percolated network (similar observation at 50 % PVA, see Fig. S2b–d). On the other hand, decreasing the PVA to 30 % yields back a matrix of PS with droplets of PVA. Overall, compared to other systems reported in the literature (e.g. polyethylene (PE)/PS [21,30], polylactide (PLA)/PS [31], etc.), the co-continuity region is quite narrow.

The interfacial tension between the two polymers, measured by the breaking thread method, gave an average value of 1.5 ± 0.3 mN/m, which is relatively low compared to the PS/high density polyethylene (HDPE) system (4.1 mN/m) [32]. However, the PVA thermal stability at the processing temperature is quite limited and the viscosity increases rapidly as a function of time. Indeed, the time sweeps reported in Fig. S1a show that the complex viscosity rapidly increases, from nearly 500 Pa s initially to over 10,000 Pa s after 60 min. As a result, measuring the zero shear viscosity (used to calculate the interfacial tension) turned out to be quite difficult. Frequency sweeps realized from low to high frequencies (Fig. S3), completed with single point measurements at low frequencies, yielded a value in-between 500-550 Pa s. The PS in contrast remained relatively stable over time (but still showing slow degradation, Fig. S1b). Since a breaking thread experiment lasted in average around 450 s (7.5 min) the viscosity of the PVA phase used for the calculation of the interfacial tension was estimated to be in-between 550 Pa s and 1000 Pa s, resulting in interfacial tension values ranging from 1.5 to 2.2 mN m. In addition, a sensitivity analysis indicated that the value of the PVA zero-shear viscosity has less impact compared to the experimental errors.

The continuity of both PS and PVA phases within the blends was next quantified by gravimetry – i.e. selective phase extraction (Fig. 3). The results support the SEM observations of Fig. 2. The PVA extraction yield is relatively low up to a content of 20 %, then increases quickly until the formation of a fully percolated PVA network at 39 % PVA (PS/PVA 61/39 vol%, indicated by the arrow). At this composition, both phases are fully continuous and form a co-continuous morphology, as is it also possible to fully extract the PS phase with chloroform. At 45 % and 50 % PVA, the PS phase still remains nearly fully continuous, but extracting the PVA phase results in very brittle samples that break very easily, indicating that the PS network is very fragile and/or tenuous. Inspection by SEM indeed shows PS droplets dispersed in a PVA matrix, linked together by very small openings linking the droplets, as observed in Fig. 2e and f (see also Fig. S2). This explains why the structure is so fragile when the PVA phase is extracted since the remaining PS droplets are linked together by very tenuous bonds.

The PS/PVA 61/39 composition showing a co-continuous morphology is adequate for the preparation of porous hydrogels: extracting the PS phase, then injecting an aqueous solution within a porous PVA mold should yield porous gels if the gelling kinetics is faster compared to the PVA solubilization rate. Based on the solubility data presented in Fig. 1, the strategy next consisted in injecting the gelling solution at low temperature, inducing rapid gelling, then extracting the PVA mold at high temperature.

PS/PVA polymer rods at a composition corresponding to the co-continuous morphology (61/39 %vol) were next melt-extruded. The objective was to develop a process allowing for the preparation of large batches of PVA molds of nearly identical features [28,29]. SEM observations (Fig. 4a) and gravimetric analysis (for the non-annealed blend) confirmed the formation of a co-continuous morphology, as it was possible to nearly fully extract both phases while maintaining sample integrity in both cases (112 % ± 2 % for the PS phase, 77 % ± 1 % for the PVA phase, indicating the presence of some PVA in the PS phase). The next step was to perform quiescent annealing over the melting temperature of PVA to let the morphology coarsen.

The SEM micrographs in Fig. 4b–f shows that the co-continuous morphology is maintained as coarsening progresses (also confirmed by gravimetric analysis as a function of annealing time), illustrating how the initially fine morphology gradually becomes coarser as the annealing time is prolonged. The alignment of the morphology in the axial (flow) direction can also be distinguished up to 20 min of annealing time. Coarsening is driven by the interfacial tension and is modulated by the viscosity of the system. Micro-CT combined with image analysis was next employed to quantify the morphological features as a function of annealing time.

The microCT analysis quantitatively shows that the morphology coarsens, with the PS and PVA domains becoming larger with annealing time (Fig. 5a–f). In addition, the PS domains are always larger compared to the PVA, a consequence of blend composition (PS/PVA 61/39 vol%). Similar results were obtained for the blends prepared with the internal mixer and annealed afterwards (Fig. S4).

Fig. 5g shows that the PS domain size increases from nearly 95 μm initially, to over 200 μm after 60 min of quiescent annealing, and from nearly 50 μm to 170 μm for the PVA domains – the morphology is already relatively coarse initially compared to the co-continuous morphology of other systems reported in the literature [19,33]. Coarsening also slows down considerably and nearly stops after 30 min of annealing time for the blends prepared in the internal mixer (Fig. S4), but it never reaches a plateau value for melt-extrusion – it could then be observed at a later time. Correspondingly, the specific interfacial area decreases from nearly 590 cm^{-1} to 95 cm^{-1} (Table S1 and S2).

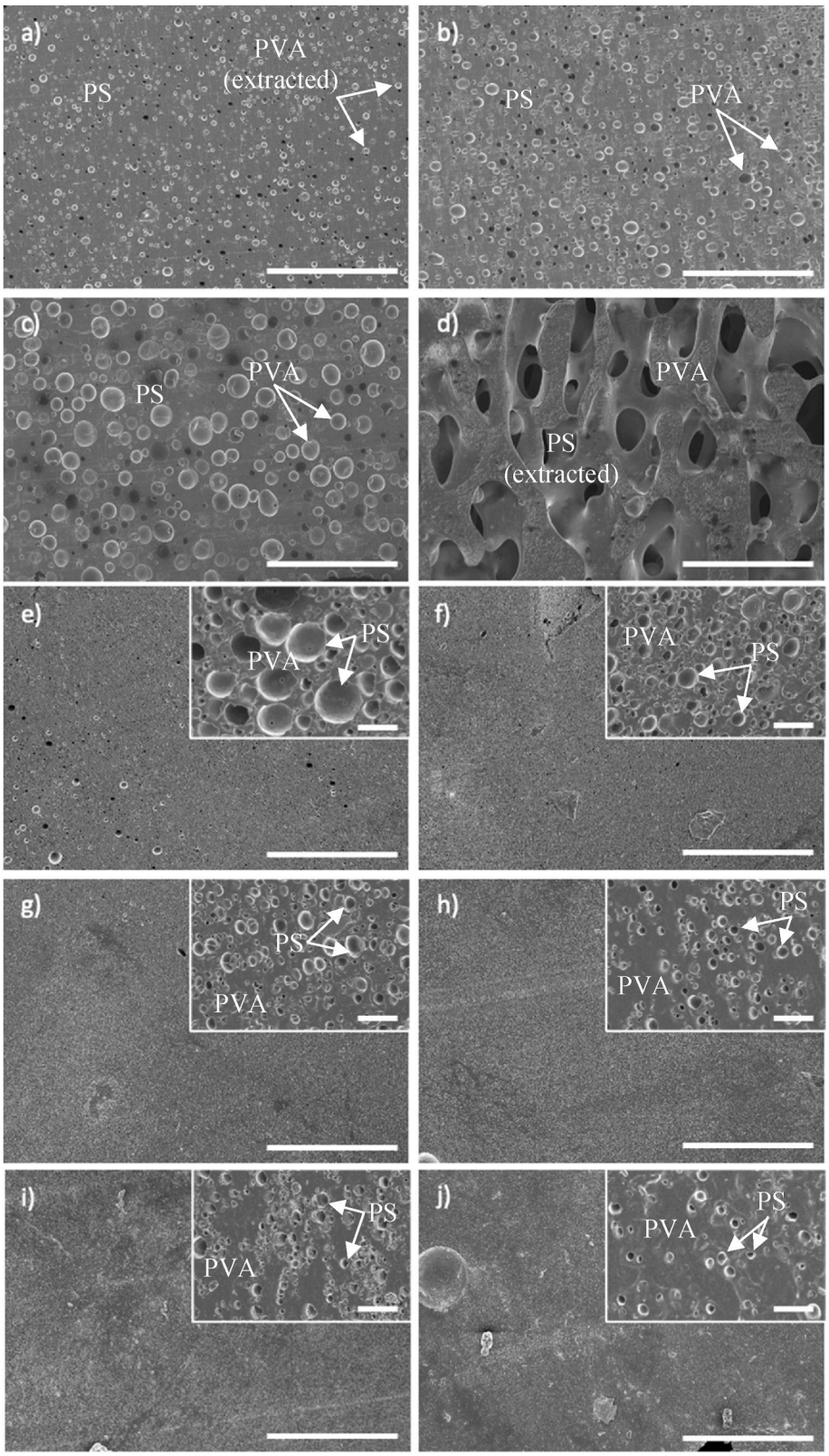

Fig. 2. Morphology of PS/PVA blends prepared in an internal mixer, after the selective extraction of PVA with water for micrographs (a) to (c), and selective extraction of PS using chloroform for micrographs (d) to (j). PS/PVA compositions in vol%: a) 90/10; b) 80/20; c) 70/30; d) 61/39; e) 60/40; f) 50/50; g) 40/60; h) 30/70; i) 20/80; j) 10/90. The white scale bars represent 100 μm for the main magnification and 2 μm for the enlarged inset images.

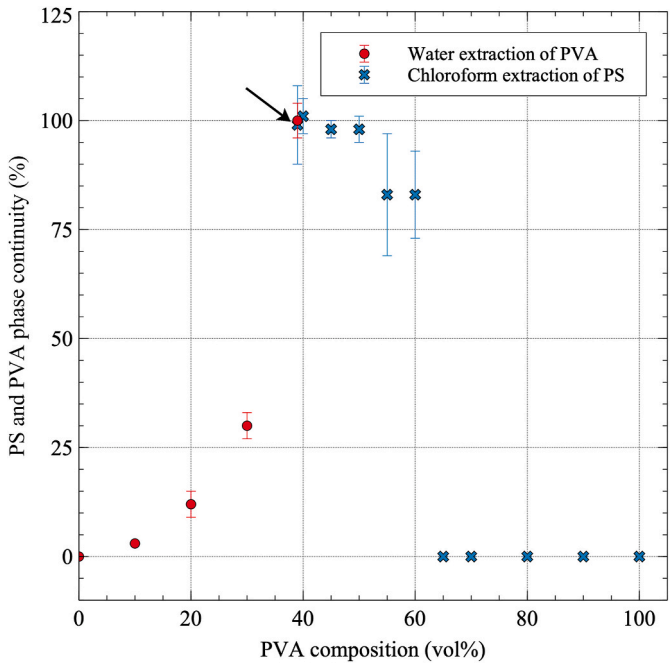

Fig. 3. Continuity of the PS and PVA phases as a function of blend composition, measured by gravimetric analysis. The arrow indicates the composition at which a co-continuous morphology is observed.

The decrease in coarsening rate, or leveling off observed after prolonged annealing, has also been observed for other polymer pairs [34, 35], but typically at a larger domain size (~1 mm). In this case here, the rapid increase in PVA viscosity, combined to the relatively low interfacial tension, could explain the decrease and leveling off of the coarsening process.

The volume fractions of the phases are 39 ± 2 vol% for PVA, and 61 ± 2 vol% for PS (pores) for annealing times ranging from 10 to 60 min. For the initial blend (no annealing), the volumetric fractions are instead 30 vol% PVA and 70 vol% PS (pores) (see Table S1 and Table S2 in SI for the complete data).

3.3. Preparation and characterization of macroporous hydrogels

The extruded rods of PS/PVA were next annealed for 30 min, trimmed by CNC machining into small cylinders, and plunged into chloroform to extract the PS phase in order to obtain porous PVA molds (Fig. 6a), with PVA domains and pore size ≈ 100 μm (Fig. 5) – typically identified as a lower limit for efficient cell colonization in a 3D biomaterial.[28] Porous hydrogels were prepared by injecting first a 4 % w/v SA solution at low temperature in the PVA molds (~5 min), i.e. near or below 2 °C. The filled molds were then plunged in a cold aqueous solution of 4 % w/v $CaCl_2$ to induce SA gelling. The molds expanded during injection and gelation (Fig. 6b) because they were submerged in a cold aqueous solution, which prevented dissolution but not swelling, as Fig. 1 displays – however, the molds expanded much less rapidly when the injection was realized at 1 °C, compared to 5 °C (Fig. S5). There is a limit to this swelling effect, since after 24 h at 5 °C, the mold reaches its maximum volume. Extended soaking beyond 24 h does not lead to further swelling. During this phase, there is minimal or no PVA extraction, with only some small parts of the edges detaching if left for too long in cold water. In addition, the colder the gelling solution is initially, the less important is the observed swelling. Finally, the PVA phase was rapidly and completely extracted in 70 °C water (within a maximum of 1 day for the tested gels, though it can take as little as 20 min depending on PVA accessibility. If a thin layer of SA gel surrounds the mold, it hinders rapid extraction due to limited accessibility of the PVA).

After PVA extraction, the porous hydrogels regain the original shape and size of the molds, with no noticeable macroscopic sample deformation (Fig. 6c). MicroCT analysis was conducted next to characterize the porosity of the resulting porous hydrogels (Fig. 7). Gel injection was tested for all annealing times. However, below 20 min of annealing, no gel could be successfully prepared. Specifically, molds annealed for 0 and 10 min could not withstand the injection process, appearing fragile and brittle even before injection at these annealing times. The injection process seemed to apply excessive pressure on the molds, occasionally causing them to fracture. In contrast, starting at 20 min of annealing time, gels could be formed without any problem.

MicroCT analysis first shows full pore interconnectivity in the hydrogels – i.e. the molding process conserves the PVA mold features (Fig. 7). The average pore size d_{pores} (128 μm) in the hydrogels is nearly 33 % higher compared to the extracted PVA domains (d_{PVA} = 96 μm) - but they still remain relatively close, and the pore size distributions overlap, as do the average PS domain size (d_{PS} = 120 μm) and average gel domains (d_{gel} = 108 μm) (Table 2). The specific surfaces of both PVA mold and porous gel are also quite comparable (157 cm^{-1} vs 198 cm^{-1}). Only the resulting pore volume fraction in the hydrogel (ϕ_{Pores} = 0.61) increases compared to the original PVA phase volume fraction (before

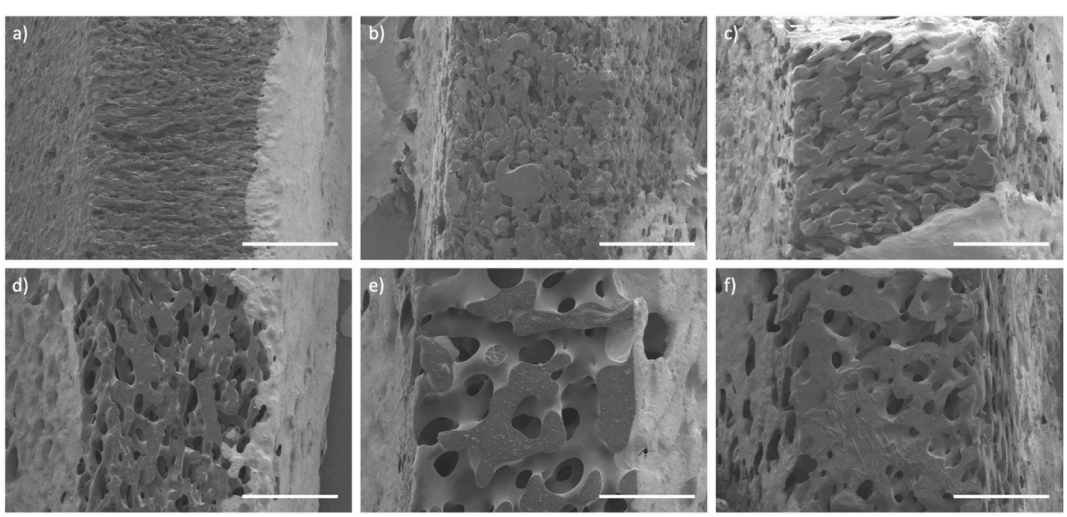

Fig. 4. Evolution of the PS/PVA 61/39 vol% blend morphology, as a function of quiescent annealing time, after the selective extraction of the PS phase with chloroform. a) No annealing, right after melt-extrusion; b) 10 min; c) 20 min; d) 30 min; e) 45 min; f) 60 min. The white scale bars represent 500 μm.

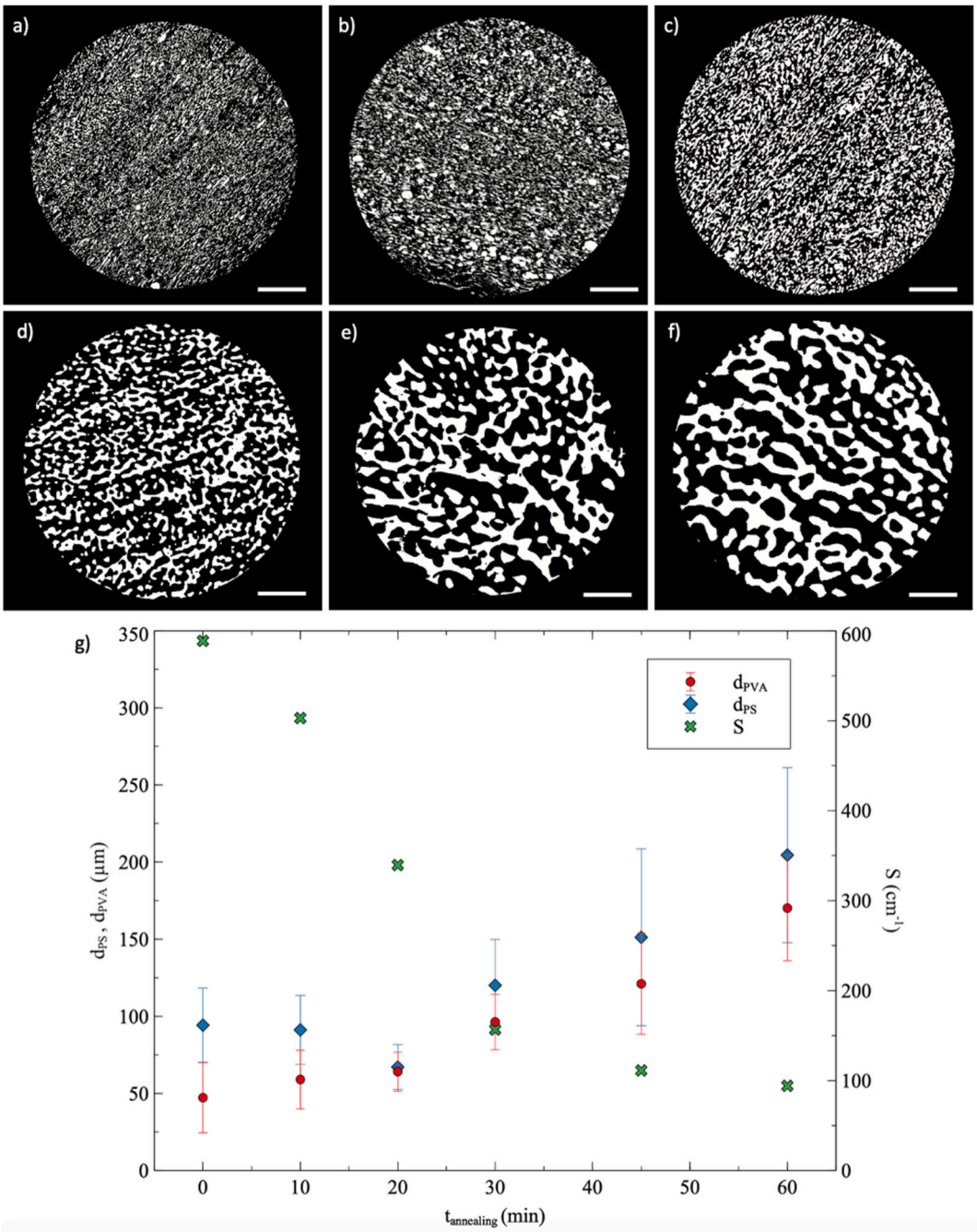

Fig. 5. (a)–(f): Evolution of the PS/PVA 61/39 vol% blend microstructure, prepared by melt-extrusion, as revealed by x-ray microtomography, as a function of quiescent annealing time. The blend was prepared by melt-extrusion, followed by quiescent annealing, CNC cutting and selective extraction of the PS phase with chloroform. a) No annealing; b) 10 min; c) 20 min; d) 30 min; e) 45 min; f) 60 min. The white scale bars represent 1 mm. White phase = PVA, black phase = pores left by PS extraction; g) Average diameter (thickness) of the PS (d_{PS}) and PVA (d_{PVA}) domains, and specific interfacial area S, as a function of quiescent annealing time $t_{annealing,}$ at T = 210 °C, for the PS/PVA 61/39 blend prepared by melt-extrusion. The data points for the diameters correspond to the average pore size of the distribution ± one standard deviation. Similar trends were obtained for the same blend composition prepared in the internal mixer (Fig. S4).

extraction, $\phi_{PVA} = 0.38$) – the opposite is observed for the gel phase volume fraction compared to the original PS phase. Whether this is due to gel syneresis, or sample preparation for microCT analysis remains to be elucidated.

To obtain a contrast between the gel phase and the pores by microCT, it is necessary to remove the free water from the pores. In Fig. 7b, extensive white domains can be seen at the edges. This is likely due either to remaining free water in the pores at the periphery, or to closed pores after removing as much water as possible with absorbent paper. These white areas were excluded during image analysis to avoid erroneous values. A deformation in shape is also noticeable (it is no longer perfectly circular), which was attributed to the softness of the hydrogel and its handling before the microCT experiment. Overall, there is a good correspondence between the microstructural features of the PVA molds, and resulting porous hydrogels, demonstrating that it is indeed possible to prepare microstructured/porous hydrogels using water-soluble polymer molds, by tuning the solubility of PVA as a function of water temperature.

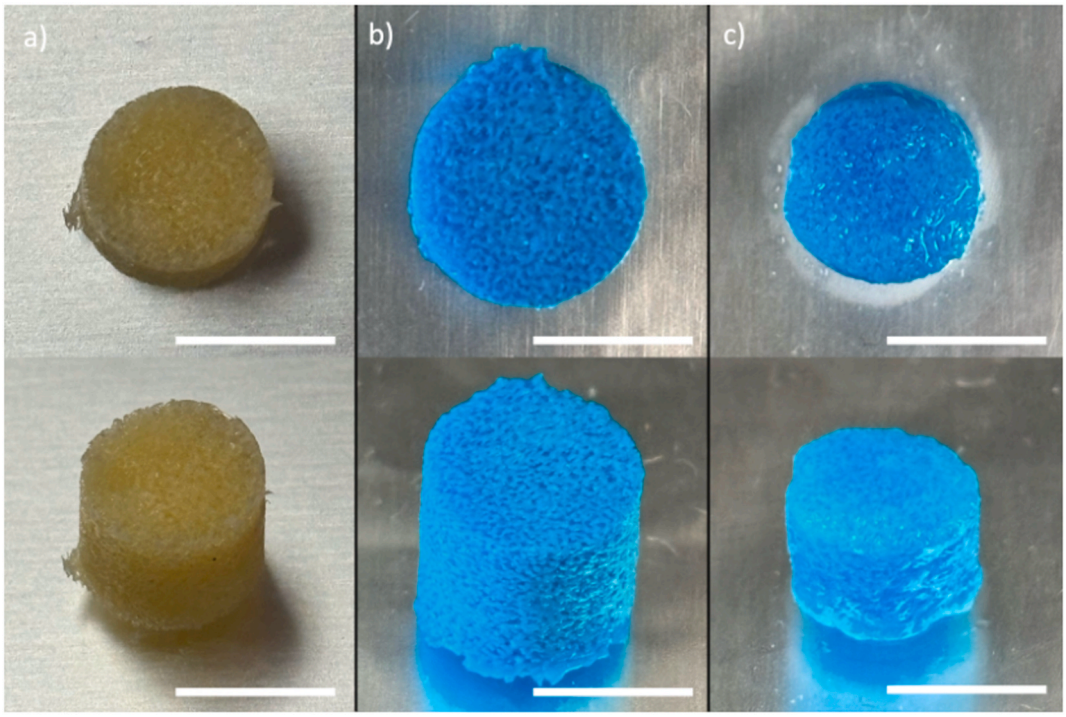

Fig. 6. Experimental steps for the preparation of a porous hydrogel composed of 4 % w/v sodium alginate (SA), with a PVA mold prepared from a PS/PVA 61/39 vol % blend annealed for 30 min (the hydrogel phase is stained with a blue food coloring dye to better distinguish the phases). The steps are as follows: a) Porous PVA mold before injection of the gelling solution, after blend annealing, CNC machining and PS extraction; b) PVA mold 24 h after the injection of the SA solution and gelation in a 4 % w/v aqueous $CaCl_2$ solution at 5 °C; c) 4 % w/v SA porous hydrogel after the extraction of the PVA mold with water at 70 °C for 1 day. The top row shows the sample from above, while the bottom row provides a top-down view. The white scale bar represents 0.5 cm. (For interpretation of the references to color in this figure legend, the reader is referred to the Web version of this article.)

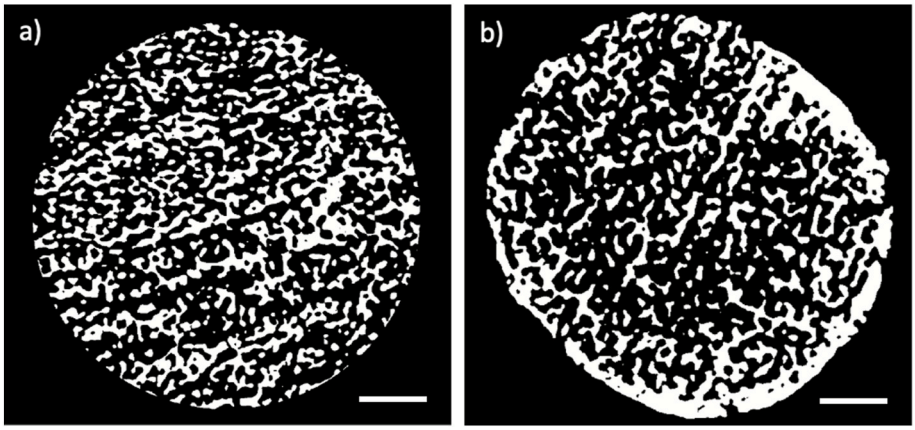

Fig. 7. a) Microstructure of a PVA mold (30 min of annealing time) viewed by microCT. White domains = PVA, black domains = porosity left by PS extraction; b) resulting macroporous alginate hydrogel (4 % w/v) once the PVA phase is extracted. White domains = SA hydrogel, black domains = porosity left by PVA extraction. The white scale bar = 1 mm.

4. Discussion

The method presented in this work allows for the preparation of water soluble polymer molds designed for the preparation of porous hydrogels for the biomedical field – i.e. for 3D cell culture, tissue engineering, etc. Using water soluble molds solves the important issue of avoiding direct contact between an organic solvent (previously used to extract the polymer molds [19,29]), the resulting hydrogel, and the seeded cells and/or tissues. Using a thermosensitive PVA also solves apparent contradicting constraints – i.e. use water soluble polymer molds to prepare water-based gels. The PVA used in this work is rather unique since it is both thermosensitive, with the possibility of tuning the solubility as a function of temperature, and melt-processable (thermoplastic PVA), allowing: (1) the preparation of large quantities of gels by using a scalable melt-extrusion process. No significant morphology variations were observed from mold to mold (both by SEM and microCT analysis) for a given quiescent annealing time (Figs. 4 and 5), indicating a robust process. In addition, porous molds with larger pores (see Fig. 6) visible by the naked eye showed no significant differences or variations either. A more systematic statistical analysis based on random sampling and microCT analysis could be realized in the future; (2) the injection and gelling of the aqueous solution at low temperature in the PVA molds (PVA is not soluble at low temperature); (3) and finally, the subsequent dissolution of the PVA molds at high temperature. To the best of our

Table 2
Comparison of the microstructural characteristics between a porous PVA mold and the resulting 4 % w/v porous alginate hydrogel, with an annealing time of 30 min.

	d_{PVA} (PVA mold)/d_{pores} (gel) (μm)	$d_{pores(PS)}$ (PVA mold)/d_{gel} (gel) (μm)	S in PVA mold/in gel (cm^{-1})	ϕ_{PVA} (PVA mold)/ϕ_{pores} (gel) (vol%)	ϕ_{Pores} in PVA mold/ϕ_{gel} in gel (vol%)
PVA mold	96 ± 18	120 ± 30	157	38	62
Porous gel	128 ± 44	108 ± 30	198	61	39

knowledge, this is the first time that such a combination of properties in PVA has been employed for such purpose. Finally, the PVA extraction step is fast and takes only a few hours, which is quicker compared to the former process using polymer molds soluble in organic solvents (a few days and up to 2 weeks) [28,29].

The process demonstrated herein also presents a number of significant advantages. For example, the PVA molds can be tuned over a broad range of average pore sizes - herein from approx. 50 μm to over 200 μm, compatible with biomedical applications requiring cell culture in 3D scaffolds [2]. In addition, the pores are fully interconnected throughout the material. However, in the case of this particular blend, the co-continuity region (or range of compositions) is quite narrow and does not allow for the tuning of the porosity volume fraction. This limitation might be due to the evolution in viscosity of the PVA phase at high temperature, and further work is required to expand the range of compositions yielding co-continuous morphologies - such as using ternary immiscible systems [36].

Li, Ma and Favis [37] have investigated the mechanisms of continuity development in binary immiscible polymer blends and have identified 3 types of systems (i.e. Types I, II and III). The PS/PVA binary system in this work possesses a low to moderate interfacial tension (1.5 mN/m) and no interfacial compatibilizer. This should correspond to the lower limit of a Type II system, in which large droplets of the minor phase first deform into threads during mixing, which then rapidly break up by capillary instabilities to form smaller droplets - until a stationary state is reached between thread formation, their break-up via capillary instability, and droplet coalescence. In Type II systems, thread lifetime is typically short due to the interfacial tension driving their break-up to form droplets, minimizing the surface energy, whereas increasing the viscosity decreases the rate of break-up. Continuity development then proceeds by droplet-droplet merging when their concentration reaches the percolation threshold. In our case, while the interfacial tension is relatively low, both the PS and PVA have relatively low viscosities, favoring short thread lifetime during mixing. This proposed mechanism is supported by the presence of both small and large droplets of PS (or PVA) at PS/PVA compositions close to the composition of the co-continuous morphology (Fig. 2), and by the breaking thread experiments, which typically took from 3 to 7 min to see the complete break up of fibers having a diameter of 50–70 μm, which is quite fast.

The viscosity increase of PVA at the processing and annealing temperature (210 °C) (Fig. S2) is accompanied by the gradual weight loss of PVA (Fig. S1) observed by TGA. PVA shows slight weight loss below 200 °C, which could be attributed to residual moisture. However, a more pronounced weight loss with temperature starts around 200 °C–210 °C, which correlates with the fast increase in complex viscosity observed by rheometry (whereas it can be attributed to the loss of a plasticizer or to thermal degradation of PVA remains to be elucidated). The processing temperature of thermoplastic PVA comes with a compromise: the melting temperature was measured at 191 °C by DSC. To ensure complete PVA melting and processability, while limiting PVA weight loss and/or degradation, extrusion was realized at 210 °C, which is 15–20 °C over the melting temperature, a standard practice. The viscosity increase of PVA however will have an impact on coarsening, by slowing down the process, which can explain why a plateau is observed during annealing for blends prepared in the internal mixer (Fig. S5). This plateau is not observed for blends prepared by extrusion and then annealed for 60 min, but prolonging the process might show it. Future experiments could look at the possibility of processing at lower temperatures closer to the melting point of PVA to limit this issue.

The strategy employed herein to prepare the porous gels involves a first injection and gelling step at a very low temperature to prevent the dissolution of the PVA molds. However, swelling of the PVA mold is still observed at 5 °C and occurs rapidly after the injection of the solution (Fig. S5). By decreasing the temperature down to 1 or 2 °C, swelling of the PVA mold is significantly slowed down, but still apparent after 24 h at 5 °C (Fig. S5). With sodium alginate, the porous gel recovers the initial mold dimensions, which is probably due to the fast gelling process in a $CaCl_2$ solution occurring by diffusion from the outer surface – swelling must then exerts an elastic deformation on the alginate, which recovers afterwards once the mold is extracted. To demonstrate the versatility of the process, macroporous hydrogels of SA and CHI chemically crosslinked with genipin and then with Ca^{2+} were also prepared, based on the protocol developed by Parès et al. [29]. The resulting macroporous gels retain the original mold dimensions (Fig. S7) and display a dark color indicative of CHI chemical crossliking with genipin – Ca^{2+} then reinforces the gels by crosslinking SA, as demonstrated by Parès et al. [29]. This demonstrates the compatibility of the process with chemical crosslinking, and also with dual/multiple crosslinking strategies. Other pathways could then be explored, such as injecting the solution at low temperature, then induce gelling and simultaneously extract the PVA mold at high temperature – this could be a valid approach for gel undergoing fast chemical crosslinking throughout the whole volume [29], or maintain the gelation phase at 1 or 2 °C to determine if a very low temperature is sufficient to prevent swelling.

Preparing porous gels with PVA molds obtained from blends annealed for 10 min or less – i.e. molds with thin PVA domains (50 μm or less, Fig. 5) – proved more difficult, as the molds rapidly became soft after solution injection and difficult to manipulate. This is probably due to the thin PVA domains (or PVA strut thickness) softening more rapidly compared to thicker domains at longer annealing times. We are still working to improve the process and solve this issue. However, the process is quite robust when the average PVA strut thickness is superior to 75 μm. Finally, since we start from a melt-processed system with a thermoplastic PVA, it is quite possible to imagine developing gels with complex shapes via a number of post-processing steps, including injection-molding or 3D printing – offering even more flexibility in terms of geometry and size.

5. Conclusion

This work demonstrates the feasibility of producing macroporous hydrogels by using a thermosensitive water-soluble thermoplastic polymer – i.e. polyvinyl alcohol (PVA) herein, avoiding the use of organic solvents directly in contact with the resulting hydrogel, and addressing a critical limitation for biomedical applications. Using melt-processed co-continuous polymer blends of polystyrene (PS) and PVA, water-soluble molds with tunable and fully interconnected pores were prepared. At a PS/PVA volume ratio of 61/39, the two immiscible polymers exhibit a co-continuous morphology that can be finely tuned via quiescent annealing. By selectively extracting the PS phase with chloroform, porous PVA molds were obtained. The unique thermosensitive properties of PVA enable low-temperature gelling solution

injection and crosslinking without mold dissolution, followed by mold removal at high temperatures to yield macroporous hydrogels. Although PVA molds exhibit some swelling at low temperatures, this does not compromise the microstructure of the resulting hydrogels, which closely retain both the original PVA molds macroscopic dimensions, and pore size of the original molds. This method offers significant potential for biomedical applications and could be adapted to other gel chemistries. Future work should explore alternative gelation and injection processes, such as high-temperature crosslinking with simultaneous mold dissolution, or maintaining molds at low temperatures without freezing to preserve structural integrity. These variations could broaden the applicability of the method to a wider range of materials and conditions, while simultaneously allowing for the preparation of large quantities of materials due to the scalable melt-extrusion method that has been employed.

CRediT authorship contribution statement

Lisa Delattre: Writing – review & editing, Writing – original draft, Validation, Methodology, Investigation, Formal analysis, Conceptualization. **Arthur Lassus:** Methodology, Investigation. **Gregory De Crescenzo:** Resources, Methodology. **Nathalie Faucheux:** Writing – review & editing, Funding acquisition. **Marc-Antoine Lauzon:** Writing – review & editing, Funding acquisition. **Benoît Paquette:** Writing – review & editing, Funding acquisition. **Mélanie Girard:** Writing – review & editing, Validation, Supervision, Conceptualization. **Nick Virgilio:** Writing – review & editing, Writing – original draft, Validation, Supervision, Resources, Methodology, Funding acquisition, Conceptualization.

Funding sources

The authors acknowledge the Fonds de Recherche du Québec – Nature et Technologie for financial support via the Projet de Recherche en Équipe program (grant number 2022-PR-299713). This work was also supported by the TransMedTech Institute (NanoBio Technology Platform) and its main funding partner, the Canada First Research Excellence Fund.

Declaration of competing interest

The authors declare that they have no known competing financial interests or personal relationships that could have appeared to influence the work reported in this paper.

Acknowledgments

The authors acknowledge Dr. Marie-Hélène Bernier (GCM Laboratory, Polytechnique Montreal) for her expertise and assistance with MicroCT experiments, Matthieu Gauthier (CREPEC, Polytechnique Montreal) for his guidance in extrusion and his invaluable laboratory support, Dainelys Guadarrama Bello (Chaire de recherche du Canada sur les tissus calcifiés et les biomatériaux et imagerie structurale, Faculté de médecine dentaire, Université de Montréal) for her assistance with SEM analyses.

Appendix A. Supplementary data

Supplementary data to this article can be found online at https://doi.org/10.1016/j.polymer.2025.128695.

Data availability

Data will be made available on request.

References

[1] A. Gopalakrishnan, S.A. Shankarappa, G.K. Rajanikant, Hydrogel scaffolds: towards restitution of ischemic stroke-injured brain, Transl. Stroke Res. 10 (1) (2019) 1–18, https://doi.org/10.1007/s12975-018-0655-6.
[2] O. Habanjar, M. Diab-Assaf, F. Caldefie-Chezet, L. Delort, 3D cell culture systems: tumor application, advantages, and disadvantages, Int. J. Mol. Sci. 22 (22) (2021) 12200, https://doi.org/10.3390/ijms222212200.
[3] V. Brancato, J.M. Oliveira, V.M. Correlo, R.L. Reis, S.C. Kundu, Could 3D models of cancer enhance drug screening, Biomaterials 232 (2020) 119744, https://doi.org/10.1016/j.biomaterials.2019.119744.
[4] T. Gancheva, N. Virgilio, Tailored macroporous hydrogels with nanoparticles display enhanced and tunable catalytic activity, ACS Appl. Mater. Interfaces 10 (25) (2018) 21073–21078, https://doi.org/10.1021/acsami.8b06560.
[5] Y. Zhao, C.-Y. Lo, L. Ruan, C.-H. Pi, C. Kim, Y. Alsaid, I. Frenkel, R. Rico, T.-C. Tsao, X. He, Somatosensory actuator based on stretchable conductive photothermally responsive hydrogel, Sci. Robot. 6 (53) (2021) eabd5483, https://doi.org/10.1126/scirobotics.abd5483.
[6] Y. Guo, G. Yu, Engineering hydrogels for efficient solar desalination and water purification, Acc. Mater. Res. 2 (5) (2021) 306–384, https://doi.org/10.1021/accountsmr.1c00057.
[7] C. Safi, A.G. Solano, B. Liberelle, H. Therriault, L. Delattre, M. Abdelkhalek, C. Wang, S. Bergeron-Fortier, V. Moreau, G. De Crescenzo, N. Faucheux, M.-A. Lauzon, B. Paquette, N. Virgilio, Effect of chitosan on alginate-based macroporous hydrogels for the capture of glioblastoma cancer cells, ACS Appl. Bio Mater. 5 (9) (2022) 4531–4540, https://doi.org/10.1021/acsabm.2c00598.
[8] T.-C. Ho, C.-C. Chang, H.-P. Chan, T.-W. Chung, C.-W. Shu, K.-P. Chuang, T.-H. Duh, M.-H. Yang, Y.-C. Tyan, Hydrogels: properties and applications in biomedicine, Molecules 27 (9) (2022) 2902, https://doi.org/10.3390/molecules27092902.
[9] Y. Ma, X. Wang, T. Su, F. Lu, Q. Chang, J. Gao, Recent advances in macroporous hydrogels for cell behavior and tissue engineering, Gels 8 (10) (2022) 606, https://doi.org/10.3390/gels8100606.
[10] R. Zhang, B. Liu, J. Ma, R. Zhu, Preparation and characterization of carboxymethyl cellulose/chitosan/alginic acid hydrogels with adjustable pore structure for adsorption of heavy metal ions, Eur. Polym. J. 179 (2022) 111577, https://doi.org/10.1016/j.eurpolymj.2022.111577.
[11] M. Dadsetan, T.E. Hefferan, J.P. Sxatkowski, P.K. Mishra, S.I. Macura, L. Lu, M. J. Yaszemski, Effect of hydrogel porosity on marrow stromal cell phenotypic expression, Biomaterials 29 (14) (2008) 2193–2202, https://doi.org/10.1016/j.biomaterials.2008.01.006.
[12] J.T. Delaney, A.R. Liberski, J. Perelaer, U.S. Schubert, Reactive inkjet printing of calcium alginate hydrogel porogens—a new strategy to open-pore structured matrices with controlled geometry, Soft Matter 6 (5) (2010) 866–869, https://doi.org/10.1039/B922888H.
[13] N. Annabi, A. Fathi, S.M. Mithieux, P. Martens, A.S. Weiss, F. Dehghani, The effect of elastin on chondrocyte adhesion and proliferation on poly (ε-caprolactone)/elastin composites, Biomaterials 32 (6) (2011) 1517–1525, https://doi.org/10.1016/j.biomaterials.2010.10.024.
[14] Y. Tang, S. Lin, S. Yin, F. Jiang, M. Zhou, G. Yang, N. Sun, W. Zhang, X. Jiang, In situ gas foaming based on magnesium particle degradation: a novel approach to fabricate injectable macroporous hydrogels, Biomaterials 232 (2020) 119727, https://doi.org/10.1016/j.biomaterials.2019.119727.
[15] I. Inci, H. Kirsebom, I.Y. Galaev, B. Mattiasson, E. Piskin, Gelatin cryogels crosslinked with oxidized dextran and containing freshly formed hydroxyapatite as potential bone tissue-engineering scaffolds, Tissue Eng. Regen. Med. 7 (7) (2013) 584–588, https://doi.org/10.1002/term.1464.
[16] I.N. Savina, M. Zoughaib, A.A. Yergeshov, Design and assessment of biodegradable macroporous cryogels as advanced tissue engineering and drug carrying materials, Gels 7 (3) (2021) 79, https://doi.org/10.3390/gels7030079.
[17] V.B. Morris, S. Nimbalkar, M. Younesi, P. McClellan, O. Akkus, Mechanical properties, cytocompatibility and manufacturability of chitosan: PEGDA hybrid-gel scaffolds by stereolithography, Ann. Biomed. Eng. 45 (2017) 286–296, https://doi.org/10.1007/s10439-016-1643-1.
[18] V. Chan, J.H. Jeong, P. Bajaj, M. Collens, T. Saif, H. Kong, R. Bashir, Multi-material bio-fabrication of hydrogel cantilevers and actuators with stereolithography, Lab Chip 12 (1) (2012) 88–98, https://doi.org/10.1039/C1LC20688E.
[19] A.-L. Esquirol, P. Sarazin, N. Virgilio, Tunable porous hydrogels from cocontinuous polymer blends, Macromolecules 47 (9) (2014) 3068–3075, https://doi.org/10.1021/ma402603b.
[20] P. Pötschke, D.R. Paul, Formation of Co-continuous structures in melt-mixed immiscible polymer blends, J. Macromol. Sci. Polym. Rev. 43 (1) (2003) 87–141, https://doi.org/10.1081/MC-120018022.
[21] Z. Yuan, B.D. Favis, Coarsening of immiscible co-continuous blends during quiescent annealing, AIChE J. 51 (1) (2005) 271–280, https://doi.org/10.1002/aic.10281.
[22] R. Oliverio, V. Patenaude, B. Liberelle, N. Virgilio, X. Banquy, G. De Crescenzo, Macroporous dextran hydrogels for controlled growth factor capture and delivery using coiled-coil interactions, Acta Biomater. 153 (2022) 190–203, https://doi.org/10.1016/j.actbio.2022.09.020.
[23] M. Kabbara, T. Gancheva, O. Gazil, N. Virgilio, Preparation of porous organogels using water soluble polymer templates, Macromol. Chem. Phys. 217 (18) (2016) 2081–2088, https://doi.org/10.1002/macp.201600212.
[24] C.A. Finch, Some properties of polyvinyl alcohol and their possible applications, in: F. C A (Ed.), Chemistry and Technology of Water-Soluble Polymers, Springer US, 1983, pp. 287–306.

[25] Y. Liu, Y. Fu, Z. Xu, X. Xiao, P. Li, X. Wang, H. Guo, Solubilization of fully hydrolyzed poly(vinyl alcohol) at room temperature for fabricating recyclable hydrogels, ACS Macro Lett. 12 (11) (2023) 1543–1548, https://doi.org/10.1021/acsmacrolett.3c00555.

[26] A.G. Solano, J. Dupuy, H. Therriault, B. Liberelle, N. Faucheux, M.-A. Lauzon, N. Virgilio, B. Paquette, An alginate-based macroporous hydrogel matrix to trap cancer cells, Carbohydr. Polym. 266 (2021) 118115, https://doi.org/10.1016/j.carbpol.2021.118115.

[27] D.C. Chappelear, Interfacial tension between molten polymers, Polym. Prepr 5 (1964) 363–371.

[28] L. Delattre, S. Naasri, A.G. Solano, H. Therriault, S. Bergeron-Fortier, V. Moreau, B. Liberelle, G. Crescenzo, M.A. Lauzon, N. Faucheux, B. Paquette, N. Virgilio, The role of pore size and mechanical properties on the accumulation, retention and distribution of F98 glioblastoma cells in macroporous hydrogels, Biomed. Mater. 19 (4) (2024), https://doi.org/10.1088/1748-605X/ad581b.

[29] L. Parès, S. Naasri, L. Delattre, H. Therriault, B. Liberelle, G. De Crescenzo, M.-A. Lauzon, N. Faucheux, B. Paquette, N. Virgilio, Macroporous chitosan/alginate hydrogels crosslinked with genipin accumulate and retain glioblastoma cancer cells, RSC Adv. 14 (48) (2024) 35286–35304, https://doi.org/10.1039/D4RA06197G.

[30] J. Li, B.D. Favis, Characterizing co-continuous high density polyethylene/polystyrene blends, Polymer 42 (11) (2001) 5047–5053, https://doi.org/10.1016/S0032-3861(00)00785-0.

[31] P. Sarazin, B.D. Favis, Morphology control in Co-continuous poly(l-lactide)/polystyrene blends: a route towards highly structured and interconnected porosity in poly(l-lactide) materials, Biomacromolecules 4 (6) (2003) 1669–1679, https://doi.org/10.1021/bm030034+.

[32] P.H.M. Elemans, J.M.H. Janssen, H.E.H. Meijer, The measurement of interfacial tension in polymer/polymer systems: the breaking thread method, J. Rheol. 34 (8) (1990) 1311–1325, https://doi.org/10.1122/1.550087.

[33] J.R. Bell, K. Chang, C.R. López-Barrón, C.W. Macosko, D.C. Morse, Annealing of cocontinuous polymer blends: effect of block copolymer molecular weight and architecture, Macromolecules 43 (11) (2010) 5024–5032, https://doi.org/10.1021/ma902805x.

[34] C.R. López-Barrón, C.W. Macosko, A new model for the coarsening of cocontinuous morphologies, Soft Matter 6 (12) (2010) 2637–2647, https://doi.org/10.1039/B926191E.

[35] M. Haji Abdolrasouli, E. Jalali Dil, J. Khorshidi Mal Ahmadi, A new empirical model for quiescent annealing of binary co-continuous polymer blends, Iran Polym. J. 30 (6) (2021) 559–568, https://doi.org/10.1007/s13726-021-00912-1.

[36] J.H. Zhang, S. Ravati, N. Virgilio, B.D. Favis, Ultralow percolation thresholds in ternary cocontinuous polymer blends, Macromolecules 40 (25) (2007) 8817–8820, https://doi.org/10.1021/ma0716480.

[37] J. Li, P.L. Ma, B.D. Favis, The role of the blend interface type on morphology in cocontinuous polymer blends, Macromolecules 35 (2002) 2005–2016, https://doi.org/10.1021/ma010104.